Bioactive Materials 6 (2021) 1175–1188

Contents lists available at ScienceDirect

Bioactive Materials

journal homepage: www.sciencedirect.com/journal/bioactive-materials

Dimethyloxallyl glycine/nanosilicates-loaded osteogenic/angiogenic difunctional fibrous structure for functional periodontal tissue regeneration

Lingling Shang, Ziqi Liu, Baojin Ma, Jinlong Shao, Bing Wang, Chenxi Ma, Shaohua Ge *

Department of Periodontology, School and Hospital of Stomatology, Cheeloo College of Medicine, Shandong University & Shandong Key Laboratory of Oral Tissue Regeneration & Shandong Engineering Laboratory for Dental Materials and Oral Tissue Regeneration, Jinan, Shandong, 250012, China

ARTICLE INFO

Keywords:
Periodontal tissue regeneration
DMOG
Nanosilicate
Osteogenesis-angiogenesis coupling
Electrospinning

ABSTRACT

The coupled process of osteogenesis-angiogenesis plays a crucial role in periodontal tissue regeneration. Although various cytokines or chemokines have been widely applied in periodontal *in situ* tissue engineering, most of them are macromolecular proteins with the drawbacks of short effective half-life, poor stability and high cost, which constrain their clinical translation. Our study aimed to develop a difunctional structure for periodontal tissue regeneration by incorporating an angiogenic small molecule, dimethyloxalylglycine (DMOG), and an osteoinductive inorganic nanomaterial, nanosilicate (nSi) into poly (lactic-co-glycolic acid) (PLGA) fibers by electrospinning. The physiochemical properties of DMOG/nSi-PLGA fibrous membranes were characterized. Thereafter, the effect of DMOG/nSi-PLGA membranes on periodontal tissue regeneration was evaluated by detecting osteogenic and angiogenic differentiation potential of periodontal ligament stem cells (PDLSCs) *in vitro*. Additionally, the fibrous membranes were transplanted into rat periodontal defects, and tissue regeneration was assessed with histological evaluation, micro-computed tomography (micro-CT), and immunohistochemical analysis. DMOG/nSi-PLGA membranes possessed preferable mechanical property and biocompatibility. PDLSCs seeded on the DMOG/nSi-PLGA membranes showed up-regulated expression of osteogenic and angiogenic markers, higher alkaline phosphatase (ALP) activity, and more tube formation in comparison with single application. Further, *in vivo* study showed that the DMOG/nSi-PLGA membranes promoted recruitment of CD90+/CD34− stromal cells, induced angiogenesis and osteogenesis, and regenerated cementum-ligament-bone complex in periodontal defects. Consequently, the combination of DMOG and nSi exerted admirable effects on periodontal tissue regeneration. DMOG/nSi-PLGA fibrous membranes could enhance and orchestrate osteogenesis-angiogenesis, and may have the potential to be translated as an effective scaffold in periodontal tissue engineering.

1. Introduction

Periodontitis is a bacterial infectious disease that affects the integrity of tooth-supporting tissues, characteristically causing gingival tissue inflammation, irreversible attachment loss, alveolar bone absorption and tooth mobility [1,2]. Currently, clinical transformation of periodontal regenerative medicine concentrating on cell therapy, signaling molecules, and biomaterials has scored some achievements [3,4]. The local administration of bioactive substances is an efficient approach for promoting periodontal tissue regeneration, and the most commonly used are growth factors or chemokines [5]. However, these bioactive proteins have some drawbacks such as short effective half-life, weak protein stability, high dosage requirements, undesired side effects, and high costs, which limit their clinical applications [6]. Alternatively, small molecule compounds or bioactive nanomaterials have emerged as novel bioactive substances for biomedical applications. In addition to superior biological effects, these bioactive substances demand small doses and have fewer side effects than high dosage growth factors due to their preferable stability in a biological environment, and thus incur relatively low cost [7]. Consequently, it is meaningful to develop a small molecule and bioactive nanomaterial-based delivery system to achieve periodontal tissue regeneration.

Dimethyloxalylglycine (DMOG), a cell-permeable small molecule, is the pharmacological inhibitor of prolyl hydroxylases (PHDs) [7]. PHDs can catalyze hydroxylation of hypoxia-inducible factor 1(HIF-1), a pivotal transcriptional factor regulating gene expression for

* Corresponding author.
E-mail address: shaohuage@sdu.edu.cn (S. Ge).

https://doi.org/10.1016/j.bioactmat.2020.10.010
Received 16 September 2020; Received in revised form 11 October 2020; Accepted 19 October 2020

angiogenesis, thereby mediating the inactivation of HIF-1. DMOG can indirectly activate HIF-1 through inhibiting PHD so as to up-regulate the genes encoding angiogenic factors, for instance, vascular endothelial growth factor (VEGF) and stromal-derived factor 1 (SDF-1) [7,8]. In recent years, as a powerful angiogenic small molecule, DMOG is highly conducive to tissue regeneration. For instance, DMOG-embedded fibrous membrane could significantly accelerate diabetic wound healing with improved angiogenesis [9,10]. By enhancing angiogenesis, various DMOG-loaded delivery scaffolds have also been demonstrated to promote bone healing [11–13]. Further, PHD inhibition can alleviate inflammatory response and exert protective effects on various inflammatory diseases [14], and DMOG attenuated the production of lipopolysaccharide (LPS)-induced inflammatory mediators in human gingival fibroblasts [15]. Therefore, DMOG may serve as a promising bioactive molecule for periodontal tissue regeneration.

Nanosilicate (nSi, $Na_{+0.7}$ $[(Mg_{5.5}Li_{0.3})Si_8O_{20}(OH)_4]_{-0.7}$), composed of bioactive silicate nanoplatelets, is a synthetic two-dimensional disk-shaped nanomaterial with diameter of 20–50 nm and height of 1–2 nm [16,17]. The nanoplatelets possess dual charge distribution, a permanent negative charge on the surface of the disks and a positive charge of the edges, which is due to the substitution of Mg^{2+} by Li^{+} [16,17]. In aqueous solutions, nSi can dissociate into nontoxic ionic products (Na^{+}, Mg^{2+}, $Si(OH)_4$, Li^{+}) which can trigger cellular responses related to tissue regeneration. Silicon is an indispensable element for growth and metabolic processes of bone tissue, and facilitates the formation and calcification of new bone tissue [18]. Orthosilicic acid ($Si(OH)_4$), a bio-absorbable form of silicon in human body, has been demonstrated to stimulate osteoblastic differentiation of osteoblast-like cells [19]. Magnesium ions induces an osteogenic effect dependent on the activation of canonical Wnt/β-catenin signaling pathway [20]. It was reported that Mg^{2+} released from Mg alloys enhanced VEGF expression in undifferentiated human bone marrow stromal cells (BMSCs), which was conducive to bone healing [21]. Mg^{2+} encouraged cellular adhesion to biomaterial surfaces, which depends on the adhesion proteins of the integrin family [22]. Li^{+} could positively regulate osteogenesis by attenuating the activity of glycogen synthase kinase-3-beta (GSK3β) and augmenting cytoplasmic β-catenin [23,24]. nSi exhibits great potential in regenerative medicine applications due to its unique properties, for instance, high-specific surface area, charged characteristics and superior bioactive performances in recent years [17]. Several studies indicated that both single nSi and nSi-based scaffolds could stimulate osteogenic differentiation of human mesenchymal stem cells (MSCs), rat BMSCs and human adipose-derived stem cells (ADSCs) [25–27]. Additionally, nSi can improve wound healing by upregulation of the VEGF pathway, enhancement of cell proliferation, and revascularization within the wound site [17]. These bioactive characteristics endow nSi with promising prospects for regenerative medicine, while its role in periodontal tissue repairing has not been explored.

Alveolar bone is highly vascularized tissue, and the vessels inside the bone can provide the crucial elements oxygen, nutrients, growth factors, and immune cells, stem cells or precursor cells for the local microenvironment in the process of periodontal tissue regeneration. Thus, osteogenesis-angiogenesis coupling process is pivotal in periodontal tissue engineering [11]. DMOG has been demonstrated to facilitate osteogenesis *in vivo*, which was mainly dependent on its angiogenic potential, whereas the intrinsic osteogenic ability of DMOG was relatively weak [6,7,13]. In addition, studies of nSi or nSi-based materials revealed the osteogenic effect [17,25–27], while they neglected the roles of osteogenesis-angiogenesis coupling in *in situ* periodontal tissue regeneration. Although the regenerative potential of DMOG or nSi was reported extensively in previous studies [9–13,17,25–27], the concept of osteogenesis-angiogenesis coupling from the two bioactive substances has not been explored in periodontal tissue regeneration. The combination of DMOG and growth factor such as BMP-2 enhanced osteogenesis in critical-sized calvarial defects [6]. Nevertheless, as mentioned above, the bioactive proteins with short effective half-life and poor protein stability require high dosage and incur high cost in case of the inactivation in the process of material preparation. By contrast, small molecule compounds or bioactive nanomaterials are more stable and economical, which are more suitable for clinical translation. Accordingly, a dual release structure based on the combination of angiogenic small molecule, DMOG and osteogenic nanomaterial, nSi was proposed to orchestrate the coupling of osteogenesis-angiogenesis and exert synergistic effects on periodontal tissue regeneration.

Poly (lactic acid-co-glycolic acid) (PLGA), a biocompatible and biodegradable polymer, has been employed for the delivery of various bioactive substances [28,29]. In this study, PLGA fibrous membranes incorporating DMOG and nSi as a co-delivery system were developed to explore their synergistic effects on periodontal tissue regeneration. The physicochemical properties, releasing profiles and cell compatibility were characterized. The *in vitro* effects on periodontal ligament stem cells (PDLSCs) was assessed by detecting osteogenic and angiogenic-related gene expression, ALP activity and tubule formation assay. *In vivo*, histological assessment, micro-computed tomography (micro-CT), and immunohistochemical analysis were used to evaluate periodontal tissue regeneration after the fibrous membranes were transplanted in a rat periodontal defect model.

2. Materials and methods

2.1. Materials

Poly (D,L-lactide-co-glycolide) (LA:GA = 75:25, MW = 90,000) was purchased from Jinan Daigang Biomaterial Co., Ltd, China. Nanosilicates (type: Laponite XLG) were supplied by Southern Clay Products, USA.

2.2. Preparation of DMOG/nSi-PLGA fibrous membranes

The PLGA-based composite membranes were fabricated by electrospinning technique. PLGA was added and stirred in hexafluoroisopropanol (HFIP, Macklin, Shanghai, China) to get the polymer solution with concentration of 20% (w/v). Then, DMOG (MCE, New Jersey, USA, 1% w/w of PLGA) and nSi (5% w/w of PLGA) were dispersed in PLGA solution and homogeneous solutions were obtained by sonicating and stirring. The spinning solution was poured into a 5 mL syringe with a metal needle. The tip of the needle calculated as 18 cm from the collector covered with aluminium foil. A voltage of 11–13 kV was applied to the syringe needle. The flow rate of the solution was 2.5 mL/h. The electrospinning process was conducted at room temperature and a relative humidity of 50%. After electrospinning, the collected composite membranes were vacuum-dried for 14 days in a desiccator to completely eliminate the organic solvent residues. Identical protocol was used to prepare the PLGA fibrous membranes with or without DMOG and nSi, which were named as PLGA, nSi-PLGA, DMOG-PLGA and DMOG/nSi-PLGA, respectively.

2.3. Physicochemical characterizations of the fibrous membranes

The morphology characteristics and structure were observed under a S-4800 scanning electron microscope (SEM, Hitachi, Japan) and a JEM-2100 transmission electron microscope (TEM, Jeol, Japan). The diameters of the fibers were measured using Nano Measure (n = 100). Chemical composition was assessed by a fourier transform infrared spectroscopy (Thermo Scientific, USA). The tensile properties of fibrous membranes (10 × 40 mm^2) were detected by the universal testing machine (Instron 3340, Boston, MA, USA). The stress-strain curves were obtained, and the tensile strength, strain at fracture and Young's modulus (E) were subsequently statistically analyzed. The hydrophobic property was detected by water contact angle measurement with a contact angle tester (DSA10, Kruss, Hamburg, Germany).

2.4. In vitro release test of the fibrous membranes

The DMOG/nSi-PLGA fibrous membranes (20 mg) were immersed in 4 mL sterile phosphate buffered saline (PBS, HyClone, Logan, Utah, USA) of a centrifuge tube placed in a constant temperature oscillator (37 °C, 100 rpm). At the desired time intervals, 2 mL PBS was extracted and equivalent fresh PBS was replenished to the tube. The absorbance of the collected PBS was measured at 208 nm wavelength using an ultraviolet spectrophotometry. The release curve of DMOG was obtained by calculating the concentration of DMOG according to the standard curve. In addition, the release profile of nSi was reflected by detecting the release of silicon (Si) using inductively coupled plasma optical emission spectroscopy (ICP-OES) analysis (iCAP 7200, Thermo Fisher Scientific).

2.5. Cell culture and cell-surface phenotype identification

The study protocol was approved by the Medical Ethical Committee of School of Stomatology, Shandong University (Protocol Number: GR201801). Human PDLSCs were derived from periodontal ligament of healthy premolars which were extracted for orthodontics. All participants signed the information consent forms based on the Helsinki Declaration.

Periodontal ligament tissues were harvested from the middle third of the root surface. The scraped tissues were digested with collagenase I (3 mg/mL, Sigma Aldrich, St Louis, MO, USA) and dispase II (4 mg/mL, Sigma Aldrich) for 40 min at 37 °C. After the digestion process was terminated, the individual cells were seeded into 25 cm^2 air-permeable flasks, and cultivated with α-minimum essential medium (α-MEM, HyClone) containing 20% fetal bovine serum (FBS, BioInd, Kibbutz, Israel) and 1% antibiotics (penicillin-streptomycin, Sigma Aldrich) in an incubator (37 °C, 5% CO_2). 80–90% confluent monolayer cells were dissociated using 0.25% Trypsin-EDTA solution (Solarbio, Beijing, China), and were then cultured with 10% FBS α-MEM containing 1% antibiotics. PDLSCs of 4∼6th generation were used for following research.

The expression of stem cell surface markers was detected by flow cytometry. Briefly, logarithmic growth phase cells were trypsinized and washed with cold PBS. The cells were incubated with blocking solution containing 1% immunoglobulin G and M for 30 min. Thereafter, the cells were labeled with monoclonal antibodies conjugated with fluorescent dyes specific for human CD29, CD44, CD90, CD34 and CD45 (BD Biosciences, New Jersey, USA) in the dark at 4 °C for 1 h. After washing, cells were subjected to flow cytometric analyses by flow cytometer (BD Biosciences).

2.6. Cytocompatibility of the fibrous membranes

The fibrous membranes were cut into circles with diameter of 15 mm in a 24-well plate, and sterilized with 75% ethanol for 1 h, followed by ultraviolet (UV) irradiation for 3 h. After washing by PBS, the fibrous membranes were soaked in α-MEM overnight. PDLSCs were inoculated to the membranes with a density of 2×10^4 cells/well. After cultivation for 3 days, cells were fixed with 4% paraformaldehyde for 10 min and then permeabilized using 0.5% Triton X-100 (Solarbio) for 10 min. After blocking with 1% bovine serum albumin (BSA, Sigma Aldrich), cells were incubated with FITC-phalloidin (Yeasen, Shanghai, China) at 4 °C overnight and nuclei were dyed by 2-(4-Amidinophenyl)-6-indolecarbamidine dihydrochloride (DAPI, Proteintech, Wuhan, Hubei, China). Cell morphology and cell adhesion to the fibers were observed under a confocal laser scanning microscope (CLSM, LSM 800, Carl Zeiss, Jena, Germany). In addition, the adhesion of cells to fibrous membranes was also observed under SEM. PDLSCs were fixed with 2.5% glutaraldehyde for 30 min and then dehydrated using graded ethanol solutions (30%, 50%, 70%, 80%, 90%, 95% and 100%) for 15 min, respectively. Subsequently, the specimens were lyophilized and observed under SEM. Cell counting kit-8 (CCK8, Dojindo Laboratories, Kumamoto, Japan) assay was performed to assess the cell viability in accordance with the manufacturer's protocols. The leaching liquors from different membranes were acquired by immersing the membranes with 10% FBS α-MEM in a constant temperature oscillator (37 °C, 100 rpm). Respectively, PDLSCs were treated with leaching liquors from different membranes for 24, 48 and 72 h. Then, the culture medium of each well was replaced with α-MEM medium with 10% CCK-8 reagent. The cells were incubated for another 2.5 h at 37 °C in the dark. The optical absorbance value at 450 nm wavelength was measured by a microplate reader (SPECTROstar Nano, BMG Labtech, Offenburg, Germany).

2.7. Alkaline phosphatase (ALP) activity assay

PDLSCs (10×10^4 cells/well) were seeded onto different fibrous membranes and cultivated using osteogenic inductive medium (OM, α-MEM containing 2% FBS, 10^{-8} mol/L dexamethasone (Solarbio), 50 mg/L ascorbic acid (Solarbio) and 10 mmol/L β-glycerophosphate (Sigma Aldrich)) for 7 and 14 days. Cells were harvested by trypsinization and lysed with 1% TritonX-100 (Solarbio) for 30 min. After collecting cell lysates by centrifugation, total protein content was determined by BCA protein assay kit (Solarbio) complying with the manufacturer's instructions. ALP activity assay kit (Nanjing Jiancheng, Nanjing, Jiangsu, China) was used to detect ALP activity on the basis of the manufacturer's specifications. The absorbance at a wavelength of 520 nm was measured by a microplate reader.

2.8. RNA isolation and quantitative real-time polymerase chain reaction (qRT-PCR)

PDLSCs (10×10^4 cells/well) were seeded to different fibrous membranes and cultivated within OM for 7, 14 and 21 days to evaluate osteogenic potential *in vitro*. Meanwhile, PDLSCs were inoculated into different fibrous membranes and cultured with endothelial cell medium (ECM, Sciencell, USA) containing 1% endothelial cell growth supplement (ECGS, Sciencell) for 7 days to assess the angiogenic differentiation ability. TRIzol reagent (Takara, Kusatsu, Japan) was used to isolate the total RNA of the cells in line with the manufacturer's instructions. The RNA concentration and purity of the samples were measured by Nanodrop 2000 ultramicro spectrophotometer (Thermo Fisher Scientific, Waltham, MA, USA). Subsequently, RNA was reverse-transcribed to complementary DNA (cDNA) using the PrimeScript® RT reagent kit with gDNA Eraser (Takara). Quantitative real-time PCR assays were performed with SYBR® Premix Ex Taq™ II (Takara) in a LightCycler 96

Table 1
Primer sequences for qRT-PCR.

Gene	Forward primer (5'∼3')	Reverse primer (5'∼3')
GAPDH	GCACCGTCAAGGCTGAGAAC	TGGTGAAGACGCCAGTGGA
Runx-2	TCCACACCATTAGGGACCATC	TGCTAATGCTTCGTGTTTCCA
OPN	TCCTAGCCCCACAGACCCTT	CACACTATCACCTCGGCCAT
OCN	TCACACTCCTCGCCCTATT	GATGTGGTCAGCCAACTCG
BSP	CCCCACCTTTTGGGAAAACCA	CCCCACCTTTTGGGAAAACCA
VEGF	GAGCCTTGCCTTGCTGCTCTAC	CACCAGGGTCTCGATTGGATG
CD31	AAGTCAAGCAGCATCGTGGTCAACAT	TTGTCTTTGAATACCGCAG
SCF	GACCTTGTGGAGTGCGTGAA	CTGGGTTCTGGGCTCTTGAAT
PLGF	TTGTCTGCTGGGAACGGCTCGT	CCGGCACACAGTGCAGATTCT

Real-Time PCR System (Roche, Basel, Switzerland) to evaluate the expression of runt-related transcription factor 2 (Runx-2), bone sialoprotein (BSP), osteopontin (OPN), osteocalcin (OCN), vascular endothelial growth factor (VEGF), CD31, stem cell factor (SCF) and placental growth factor (PLGF) in gene level. The primers sequences of the target genes and the housekeeping gene glyceraldehyde-3-phosphate dehydrogenase (GAPDH) for qRT-PCR were presented in Table 1.

2.9. Tubule formation assay

PDLSCs (10×10^4 cells/well) were seeded onto different fibrous membranes and cultured with ECM for 14 days. Cell tubule formation assay was carried out according to the guide of manufacturer's specifications. The basement membrane Matrigel (Corning, Corning, New York, USA) was unfrozen at 4 °C overnight and coated on the pre-cooling 48-well plates (100 μL/well) at 37 °C for 30 min. During solidification, cells were trypsinized and collected. Afterwards, cells (5×10^4 cells/well) were inoculated into Matrigel-coated 48-well plates. After incubation for 6 h at 37 °C, the cells were observed under a microscope (OLYMPUS IX73, Tokyo, Japan) to assess the tube formation ability. Images of the tubular structures were captured, and the important parameters of angiogenesis, including number of nodes, segments, meshes and total length were quantified with Image J 1.44 software (NIH, Bethesda, Maryland, USA).

2.10. Rat periodontal defect model preparation

Wistar rats (male, 8 weeks, SPF, Beijing, China) were used in this study (n = 6). This study was approved by the Medical Ethics Committee of School of Stomatology, Shandong University, Jinan, China (Permit Number: GD201801). The operation on rats was based on the guidelines of the Care and Use of Laboratory Animals of the Chinese Science and Technology Ministry. The surgical operation was conducted under pentobarbital sodium anesthesia (40 mg/kg body weight).

A mandibular buccal bone defect ($5 \times 4 \times 1$ mm^3 L × H × D) was created with a dental drill. The critical bone defect was situated approximately 1 mm distal to the anterior margin of the mandible, and the coronal margin of bone defect was 1 mm apical to the crest of the alveolar bone. The rats were randomly assigned to five groups and different membranes were implanted into the defects: (1) no treatment (negative control, NC) (2) PLGA, (3) nSi-PLGA, (4) DMOG-PLGA, and (5) DMOG/nSi-PLGA. At 1, 2, 4, 8 weeks postoperatively, the rats were sacrificed by excessive pentobarbital anesthesia and fixed with 4% paraformaldehyde by cardiac perfusion. The mandibles of the rats were collected for the following experiments.

2.11. Micro-computational tomography (micro-CT) analysis

A micro-CT (PerkinElmer, Baesweiler, Germany) was applied to scan the specimens to analyze bone remodeling *in vivo*, with scan settings of voltage 90 kV, current 88 μA and voxel resolution 50 μm at 360°. CT vox and CT analysis software were used to reconstruct the images for 3D visualization and analysis. Quantitatively, several indexes including the percentage of bone volume (bone volume/tissue volume, BV/TV), trabecular thickness (Tb.Th) and trabecular separation (Tb. Sp) were analyzed and calculated to assess of bone regeneration.

2.12. Histological analysis

The fixed samples were decalcified using disodium ethylenediamine tetraacetate (EDTA, 10%) for 1 month at 4 °C. Afterwards, the specimens were dehydrated within a graded series of ethanol solutions. After vitrification with dimethylbenzene, the specimens were embedded in paraffin to incise transverse section (5 μm thickness) of the osteochondral defect area. Hematoxylin and eosin (H&E) staining and immunohistochemical staining for ALP (Abcam, Cambridge, UK), Runx-2 (Abcam), collagen-I (Col-I, Abcam), CD31 (Abcam) and alpha-smooth muscle actin (α-SMA, Abcam) were performed to appraise periodontal tissue regeneration in line with the manufacturer's protocols. Immunofluorescence double staining for CD90 (Abcam) and CD34 (Abcam) was performed to detect CD90+/CD34− stromal cells, and cell nuclei were stained with DAPI (Solarbio). To evaluate osteoclastogenesis, tartrate-resistant acid phosphatase (TRAP) staining was conducted to identify TRAP positive cells with a leukocyte acid phosphatase kit (Solarbio) according to the manufacturer's protocols. The staining of specimens was viewed with a microscope (Olympus, BX53). The number of CD90+CD34− stromal cells, TRAP-positive cells, Runx-2-positive cells and the area of newly formed bone were counted and calculated, and mean optical density (OD) of Col-I and ALP staining was measured by the Image pro-plus 6.0 software (Media Cybernetics, Silver Spring, MD, USA). The angulations of newly formed fibrous ligament tissues to root surfaces was measured using Image J 1.44 (NIH).

2.13. Statistical analysis

Data were shown as mean ± standard deviation (SD). Variances between more than two groups were compared by one-way ANOVA followed by Tukey HSD comparison test, and differences between two groups were analyzed by two-way *t*-test using GraphPad Prism software (version 6, by MacKiev Software, Boston, MA, USA). $P < 0.05$ was set as statistically significant difference.

3. Results

3.1. Physicochemical characterization of the fibrous membranes

The surface morphology of the membranes was characterized by SEM (Fig. 1A–H). Inserts of Fig. 1A–E were the gross photographs of four membranes. The membranes showed staggered fibrous structure. All of the fibers possessed uniform and smooth morphology without beads or broken strands, and the mean diameters were 1069 nm (PLGA), 953.30 nm (nSi-PLGA), 1080.933 nm (DMOG-PLGA) and 921.62 nm (DMOG/nSi-PLGA), respectively. We found that incorporation of DMOG almost had no effect on the diameter of PLGA fibers, while nSi could slightly decrease the diameter. The EDS mapping (Fig. S1A) and spectrum (Fig. S1B) identified the element composition and content of nSi, and therein the element content of Na, Mg and Si was 0.23%, 15.89% and 29.11%, respectively. TEM image of nSi exhibited a nanodisk-like geometry with the diameter of about 50 nm (Fig. S1C). In addition, TEM result of nSi-PLGA membrane showed that nSi (yellow arrow) could be seen in the single fiber, indicating that nSi was successfully embedded into PLGA (Fig. S1D).

The FTIR spectra were obtained to confirm the characteristic functional groups and surface chemical properties (Fig. 1I). The peaks at 2995 cm^{-1} and 2946 cm^{-1} were separately due to $–CH_3$ and –CH vibrations. The strong absorption peak at 1746 cm^{-1} was attributed to the carbonyl –C═O stretching vibration. Two peaks at 1180 and 1083 cm^{-1} were corresponding to the –C–O stretching vibrations of the ester group. In addition, the peak at 1452 cm^{-1} was ascribed to $–CH_2$ bending vibration, and the peaks at 990 and 685 cm^{-1} belonged to the –CH bending vibrations [30,31]. The characteristic peaks of these four membranes resembled those of the raw PLGA meaning that the surface chemical properties are unaffected by the electrospinning process.

The mechanical performances of the fibrous membranes were assessed by tensile testing. Representative tensile stress-strain curves of different membranes were shown in Fig. 1J, and the Young's modulus (E), ultimate tensile strength and the strain at fracture were statistically analyzed and summarized in Table 2 presented as mean ± standard deviation. Compared with PLGA and DMOG-PLGA samples, the samples containing nSi exhibited significant augmentation for the tensile strength and the Young's modulus. The tensile strength of nSi-PLGA and DMOG/nSi-PLGA membranes was 2.70 ± 1.72 and 2.85 ± 0.21 MPa respectively, which were approximately three-fold compared to PLGA

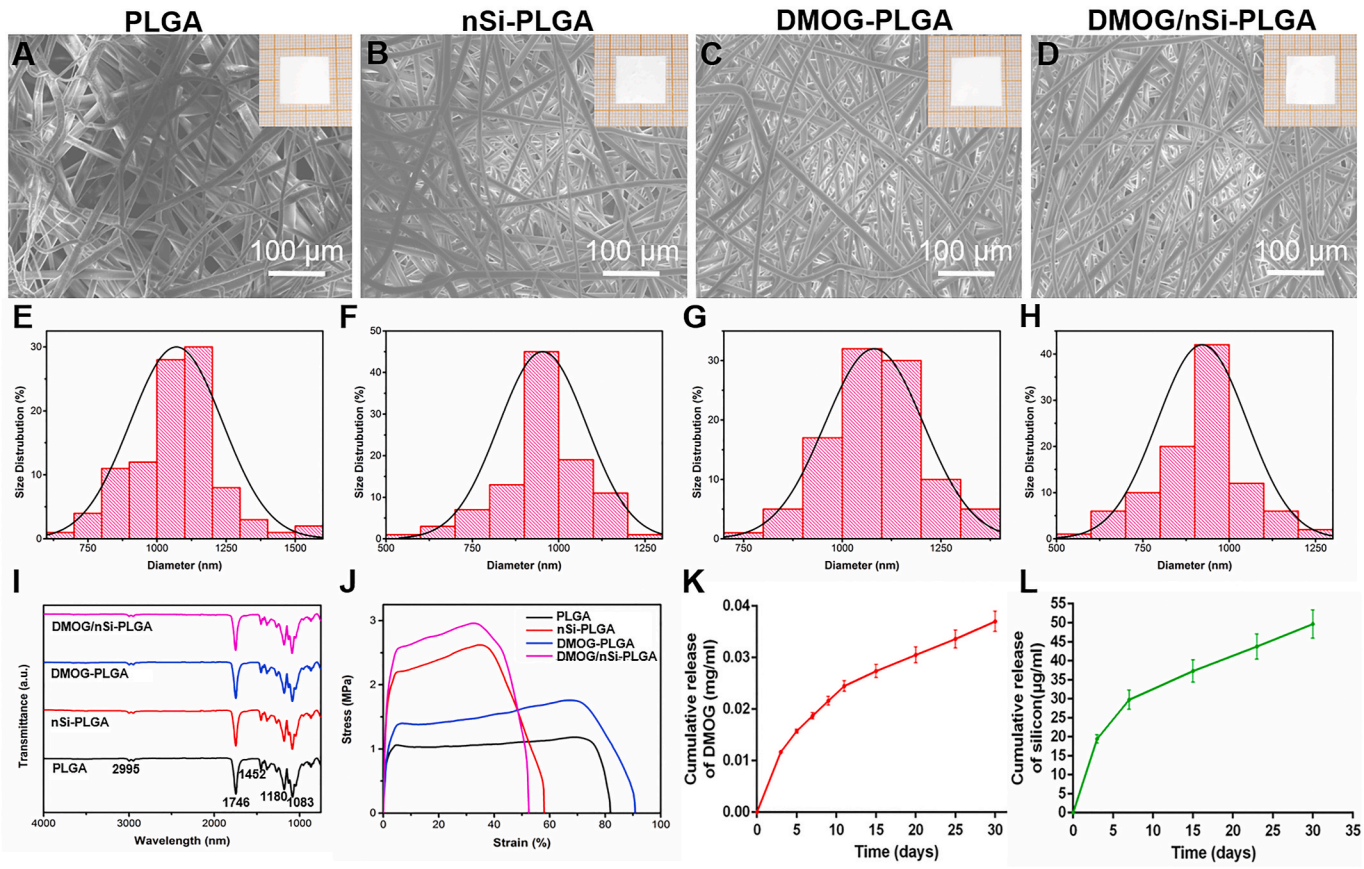

Fig. 1. Characterization of the fibrous membranes. (A–D) SEM images and gross photographs (insert) of different fibrous membranes. (E–H) Diameter distribution analysis of different fibrous membranes. Scale bars = 100 μm. (A,E) PLGA, (B,F) nSi-PLGA, (C,G) DMOG-PLGA, (D,H) DMOG/nSi-PLGA. (I) FTIR spectra of the fibrous membranes. (J) Stress-strain curve of different fibrous membranes. (K,L) Cumulative release curves of DMOG and silicon from DMOG/nSi-PLGA fibrous membrane.

membrane (0.97 ± 0.23 MPa). However, the elongation at break of nSi-embedded membranes was reduced to 56.32 ± 15.86% and 55.22 ± 3.933% in comparison to PLGA (75.88 ± 8.427%).

The controlled releasing capacity of the polymeric fibers was evaluated by detecting *in vitro* release of DMOG and silicon. The accumulated concentration profile of DMOG released from DMOG/nSi-PLGA membrane was illustrated in Fig. 1K, and DMOG exhibited an initial burst release at the first 72 h. Gradually, the releasing rate slowed down while DMOG was still sustainably released from the membranes up to 30 days with the accumulated concentration of 0.035 mg/mL. The cumulative releasing concentration of silicon was presented in Fig. 1L. Similar to the release profile of DMOG, silicon was also continuously released from the membranes, with an explosive release at the first 72 h and an accumulated concentration of 50 μg/mL at 30 days.

The water contact angle of the membranes was measured to evaluate surface wettability of the polymers and the results were shown in Fig. S2. The contact angle of PLGA fiber was 138.1 ± 0.32°. The addition of DMOG and nSi could improve the hydrophilicity of the polymer fibers and the contact angle of the fibrous membranes decreased to 127.4 ± 3.62° after incorporation of the two bioactive substances ($P < 0.05$).

Table 2
Mechanical properties of fibrous membranes.

Sample	Tensile strength (MPa)	Strain at fracture (%)	Young's Modulus (MPa)
PLGA	0.9667 ± 0.2255	75.88 ± 8.427	1.127 ± 0.3630
nSi-PLGA	2.700 ± 1.720	56.32 ± 15.86	1.997 ± 0.6870
DMOG-PLGA	1.850 ± 0.07071	86.51 ± 6.040	1.085 ± 0.2192
DMOG/nSi-PLGA	2.850 ± 0.2121	55.22 ± 3.933	2.205 ± 0.2333

3.2. Cytocompatibility of the fibrous membranes

The effect of material surface microstructure on cell behavior was assessed by observing the adhesion and morphology of PDLSCs on the surfaces of the fibrous membranes under CLSM and SEM. Cell morphology on different membranes was reflected by cytoskeleton (F-actin) staining at the third day (Fig. 2A–E). PDLSCs attached to all the membranes and spread over the fibers with elongated cytoskeleton in comparison with cells on tissue culture plate (TCP). In addition, cell density on the surface of TCP and four fibrous membranes was roughly equivalent, indicating that the membranes with or without DMOG and nSi had no adverse effect on cellular adhesion and growth. Further, the interface state of cells and membranes was observed under SEM after cultivation for 3 days (Fig. 2F–I). In accordance with cytoskeleton staining, PDLSCs adhered stably to the membranes and stretched entirely over the surfaces of the membranes by pseudopods. Additionally, CCK-8 assay was conducted to evaluate the cytotoxic effect of released bioactive substances. As shown in Fig. 2J, after cultivation for 1, 2 and 3 days, PDLSCs showed high viability, and there was no significant difference among all the membranes. Therefore, the membranes were biocompatible and could serve as a compatible attachment surface for cell growth.

3.3. Osteogenic differentiation potential of PDLSCs on DMOG/nSi-PLGA fibrous membranes in vitro

Flow cytometric analysis demonstrated that PDLSCs positively

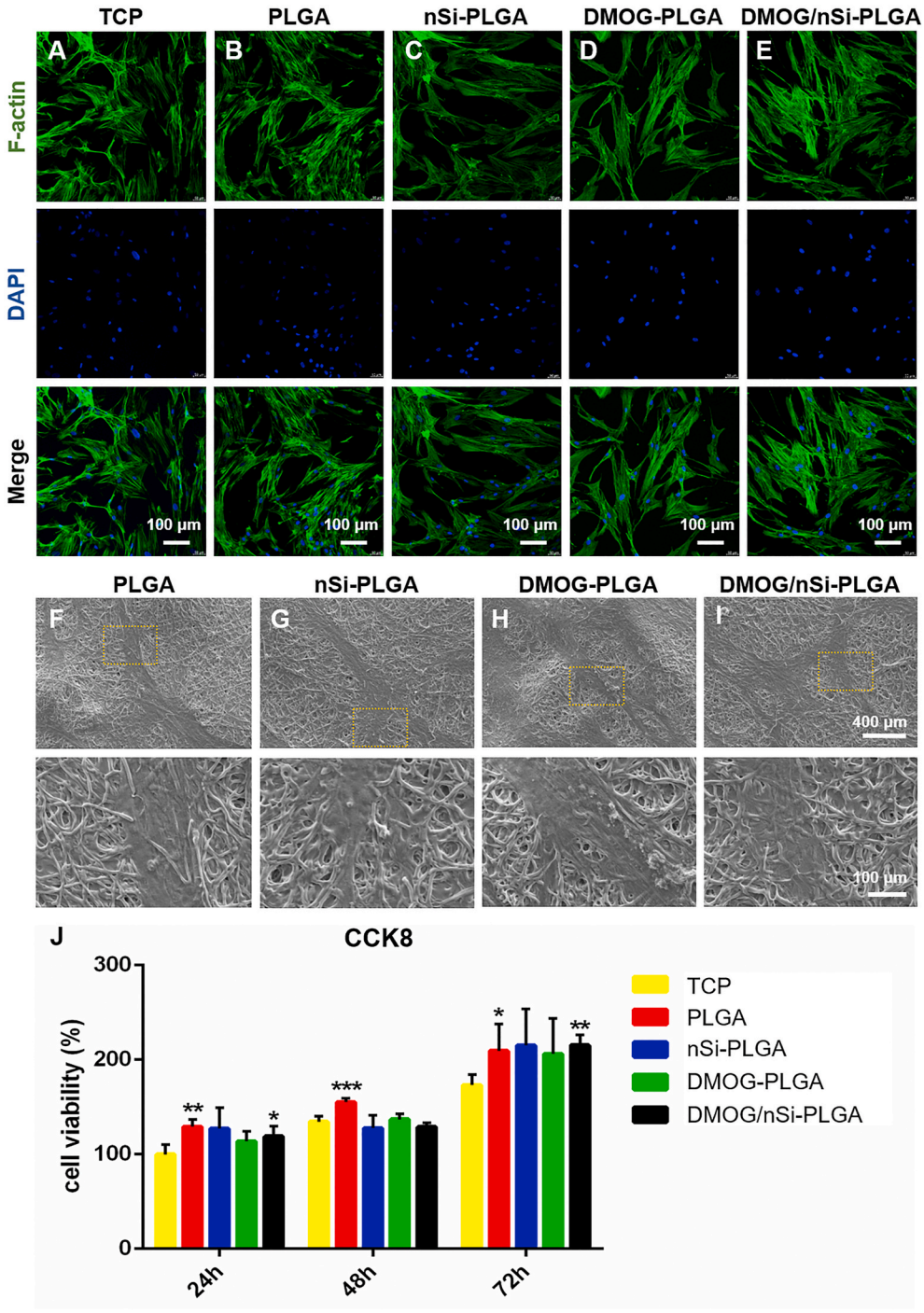

Fig. 2. Cytocompatibility assessment of the fibrous membranes. (A–I) Cell morphology on the fibrous membranes after cultured for 72 h. (A–E) Cytoskeleton staining (green) by FITC-phalloidin, and nucleus (blue) by DAPI. Scale bars = 100 μm. (F–I) Different magnifications of cellular SEM images on different fibrous membranes. Scale bars = 400 μm or 100 μm. (J) Cell viability after cultivation with or without leach liquor from different fibrous membranes. $*p < 0.05$, $**p < 0.01$ and $***p < 0.001$ compared with TCP.

expressed MSCs markers CD44, CD29, and CD90, and negatively expressed hematopoietic stem cells markers CD34 and CD45 (Fig. S3). Osteogenic differentiation is a pivotal aspect for periodontal tissue engineering. PDLSCs were seeded on the four different membranes for 7, 14 and 21 days to explore osteogenic differentiation potential of DMOG/nSi-PLGA fibrous *in vitro*. ALP activity was detected at day 7 and 14, respectively. The results showed that DMOG/nSi-PLGA fibrous membrane significantly enhanced ALP activity as compared to the membranes with no or single stimulus in the early period of osteogenic induction (Fig. 3A and B, $P < 0.01$). Further, qRT-PCR was performed to detect mRNA levels of osteogenic genes, Runx-2, OPN, OCN and BSP at day 7, 14 and 21 (Fig. 3C–F). Compared with NC and PLGA group, nSi-PLGA group significantly up-regulated the mRNA levels of osteogenic genes, and gene level of nSi-PLGA group was higher than that of DMOG-PLGA group. By contrast, DMOG/nSi-PLGA group presented the highest gene levels of osteogenesis-related markers among all groups at specific time points although there was no statistical difference for Runx-2 and OPN at day 7.

3.4. Angiogenic ability of PDLSCs on DMOG/nSi-PLGA fibrous membranes in vitro

Tube formation assay was performed to assess the angiogenic capacity of PDLSCs on different membranes. Capillary-like networks were formed by PDLSCs in all groups after 6 h cultures on the Matrigel. DMOG-PLGA membranes effectively stimulated tube formation. However, PDLSCs

cultured on DMOG/nSi-PLGA membranes generated more obvious tube structures than those cultured on DMOG-PLGA membranes (Fig. 3G–J). The analysis results showed that cells cultured on DMOG/nSi-PLGA membranes generated the highest number of nodes, segments, meshes and the total tube length among all groups (Fig. 3K-N, $P < 0.05$). In addition, angiogenic effect of DMOG/nSi-PLGA fibrous membranes was further evaluated by detecting the angiogenesis-related genes expression including VEGF, CD31, SCF and PLGF (Fig. 3O–R). In line with tube formation assay, mRNA levels of the angiogenesis-related genes for cells cultured on DMOG/nSi-PLGA membranes was significantly up-regulated compared with that of the other groups ($P < 0.05$). Consequently, DMOG/nSi-PLGA fibrous membranes was in favor of angiogenesis *in vitro*.

3.5. Stromal cells recruitment effect of DMOG/nSi-PLGA fibrous membranes

DMOG/nSi-PLGA fibrous membranes were implanted into the mandibular defects of rats, and the surgical procedure was presented in Fig. S4. CD90+/CD34− cells were detected by immunofluorescent double staining for CD90 (green) and CD34 (red) to assess the reaction of host stromal cells to DMOG and nSi during tissue repair (Fig. 4). We found that the number of stromal cells for NC and PLGA groups was obviously smaller than that for the other groups, and DMOG/nSi-PLGA group recruited most stromal cells to periodontal defect in the early tissue repairing process ($P < 0.001$). At day 7, more stromal cells were observed in DMOG/nSi-PLGA group in contrast to other groups ($P < 0.001$). nSi-PLGA and DMOG-PLGA groups recruited more stromal cells than NC and PLGA groups ($P < 0.001$). At day 14, the number of stromal cells generally reduced for all groups in comparison with day 7, whereas DMOG/nSi-PLGA group still had the most numerous CD90+CD34− stromal cells among all groups ($P < 0.001$). At day 28, the number of CD90+CD34− stromal cells was reduced significantly, and there was no significant difference among all groups ($P > 0.05$). Thus, DMOG/nSi-PLGA membrane promoted stromal cells migration in periodontal defects at early phase of tissue healing.

3.6. Effect of DMOG/nSi-PLGA fibrous membranes on revascularization in vivo

The immunohistochemical staining was performed to detect the expression of angiogenesis-related markers α-SMA (Fig. 5A) and CD31 (Fig. 5B). At week 1 and 2, nearly no positive staining was seen in NC and PLGA groups, and low expression presented in nSi-PLGA group. The angiogenic markers were highly expressed in DMOG-PLGA and DMOG/nSi-PLGA groups, whereas the positive brown staining with the typical round or oval structure was more obvious in DMOG/nSi-PLGA group. At week 4, the round or oval positive staining decreased significantly, and there was no statistical difference among all groups. Consequently, DMOG/nSi-PLGA membrane could enhance revascularization *in vivo* at early wound healing.

3.7. Effect of DMOG/nSi-PLGA fibrous membranes on osteoclastogenesis

Osteoclast activity was detected by TRAP staining (Fig. 5C,E). At week 1, TRAP+ cells were abundant and mainly located in the margin of bone trabecular. More TRAP+ cells were found in nSi-PLGA, DMOG-PLGA and DMOG/nSi-PLGA groups than that in NC and PLGA groups ($P < 0.05$), while DMOG/nSi-PLGA group exhibited the most abundant TRAP+ cells among all groups ($P < 0.05$). At week 2, TRAP+ cells decreased significantly, and there was no significant difference among all groups ($P > 0.05$). Thereafter, at week 4, TRAP+ cells were scarcely observed in all groups. Thus, DMOG/nSi-PLGA membrane could stimulate early transient osteoclastogenesis.

3.8. Effect of DMOG/nSi-PLGA fibrous membranes on periodontal defect repair and regeneration

Micro-CT, histomorphological assessment and immunohistochemical analysis were used to confirm the *in vivo* osteogenesis effect of DMOG/nSi-PLGA fibrous membranes on periodontal defect repair. The specimens were scanned 1, 2, 4, and 8 weeks after surgery for mandibular bone remodeling analysis by micro-CT. The representative 3D digital reconstructed images indicated that DMOG/nSi-PLGA group presented a greater degree of bone defect healing and the bone defect was filled with more newly formed calcified tissue than the other groups for all time points. During bone reconstruction, the newly formed calcified tissue gradually increased and the defect of DMOG/nSi-PLGA group was completely filled with new tissues at week 8 (Fig. 5D). Further, quantitative analysis of the reconstructed images was conducted to calculate several indexes from ROI. In accordance with the 3D images, the percentage of bone volume (BV/TV) increased for all groups as time progresses while DMOG/nSi-PLGA group had the highest BV/TV level among all groups at week 1, 2, 4 and 8 (Fig. 5F, $P < 0.01$), which suggested that more new bones formed in this group. In addition, the trabecular bone thickness (Tb.Th) of DMOG/nSi-PLGA group dramatically augmented at week 2, 4, 8 (Fig. 5G, $P < 0.01$), and simultaneously, trabecular separation (Tb.Sp) decreased in comparison with other groups at week 4 and 8 (Fig. 5H, $P < 0.05$), which implied that the newly formed bones were much more mature and denser in DMOG/nSi-PLGA group. We also found that DMOG-PLGA group had some effect on bone repair, and nSi-PLGA group acquired more newly formed bone than NC and PLGA groups.

The effect of DMOG/nSi-PLGA fibrous membranes on periodontal bone regeneration were further confirmed with H&E staining (Fig. S5). At week 1 after surgery, there was almost no bone in the defects of NC group. The bone defect area was not observably reduced and only small amount of new bone formation was found on the edge of the defects in four fibrous membrane groups, and DMOG/nSi-PLGA group had more newly formed bone tissues ($P < 0.01$). At week 2, more new bones were observed in the defects of all groups than week 1. nSi-PLGA and DMOG-PLGA groups presented more new bones as compared to other two groups without the bioactive substances, while DMOG/nSi-PLGA group showed the most abundant bones among all groups. At week 4, the defect area of all groups significantly decreased and DMOG/nSi-PLGA group still induced more bone formation than the other groups. At week 8, the defects were nearly filled with newly formed bones and DMOG/nSi-PLGA group possessed more mature and dense bones than the other groups.

Further, the expression of bone specific matrix proteins was detected by immunohistochemical staining to evaluate the osteogenesis effect. ALP expression in DMOG/nSi-PLGA group was the highest among all groups at early stage (Fig. S6, $P < 0.05$). At week 8, the expression of ALP reduced significantly, and there was no statistical difference among all groups ($P > 0.05$). By contrast with the other groups, Runx-2+ cells significantly increased in DMOG/nSi-PLGA group at week 1 and 2 (Fig. S7, $P < 0.01$). At week 4 and 8, Runx-2+ cells decreased obviously and were hardly observed in all groups. The expression of Col-I increased gradually over the research intervals, and exhibited the highest level in DMOG/nSi-PLGA group (Fig. S8, $P < 0.01$) even though nSi-PLGA and DMOG-PLGA groups also presented high expression of Col-I in comparison with NC and PLGA groups ($P < 0.01$). Thus, the collaborative application of the two factors acquired the greatest extent of bone regeneration.

3.9. Effect of DMOG/nSi-PLGA fibrous membranes on periodontal ligament and cementum regeneration

The fiber bundle angles of newly formed periodontal ligament against the root surfaces were measured to quantitatively analyze the fiber alignment (Fig. 6A). The angulation of the native mature ligament was 48.21° (Fig. 6B), and the fiber angulation of periodontal ligament in

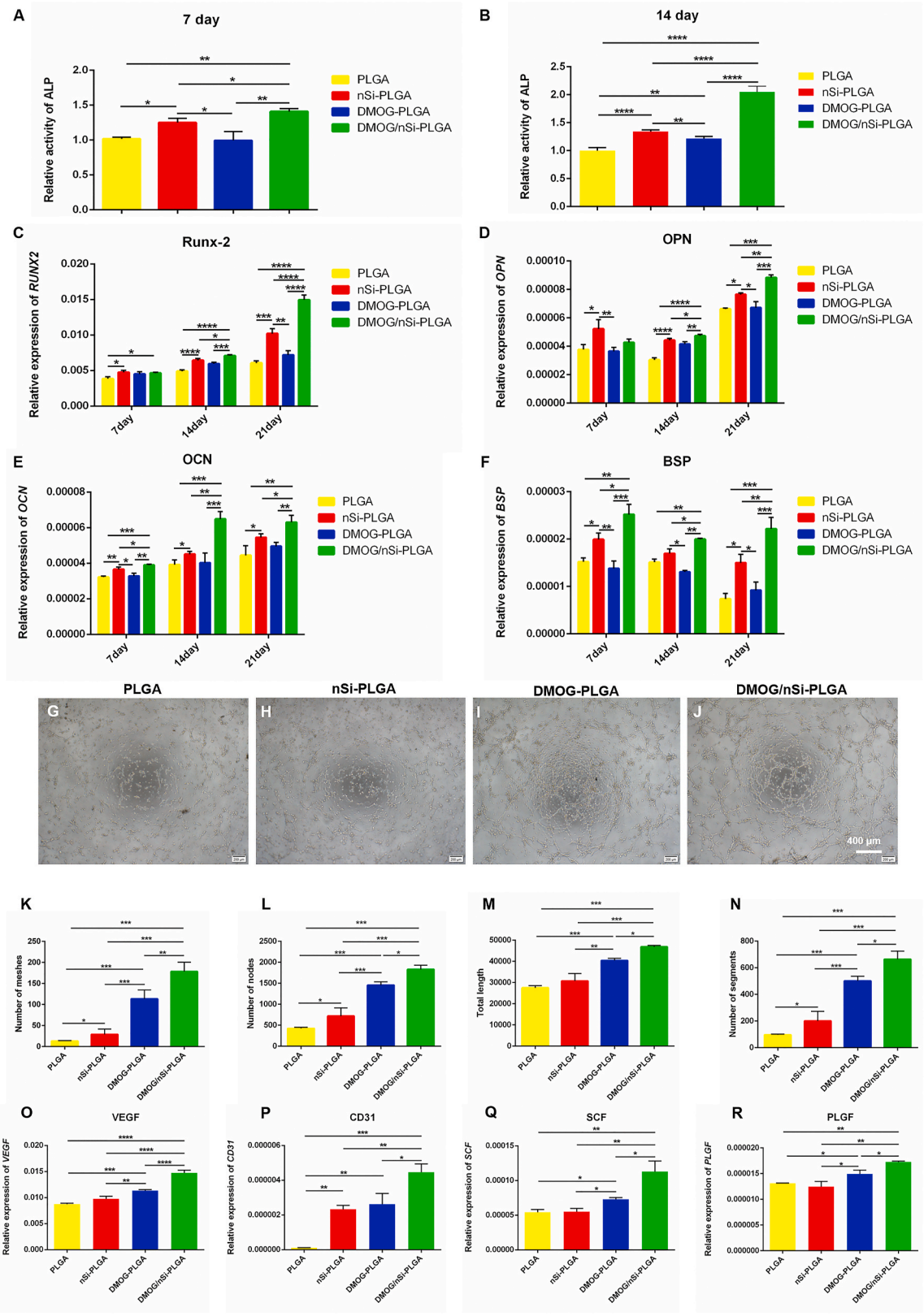

Fig. 3. Osteogenic and angiogenic differentiation of PDLSCs on different fibrous membranes. (A,B) ALP activity at day 7 and 14. (C–F) qRT-PCR analysis for the relative mRNA levels of Runx-2 (C), OPN (D), OCN (E) and BSP (F) after cultured for 7, 14 and 21 days. (G–J) Representative images of tubule formation assay of PDLSCs cultured on different fibrous membranes. Scale bars = 400 μm (K–N) Quantitative analysis of number of nodes (K), number of segments (L), number of meshes (M) and the total tube length (N) of the formed tubules. (O–R) qRT-PCR analysis for the relative mRNA levels of angiogenesis-related gene VEGF (O), CD31 (P), SCF (Q) and PLGF (R) after cultured for 7 days. *$p < 0.05$, **$p < 0.01$, ***$p < 0.001$ and ****$p < 0.0001$.

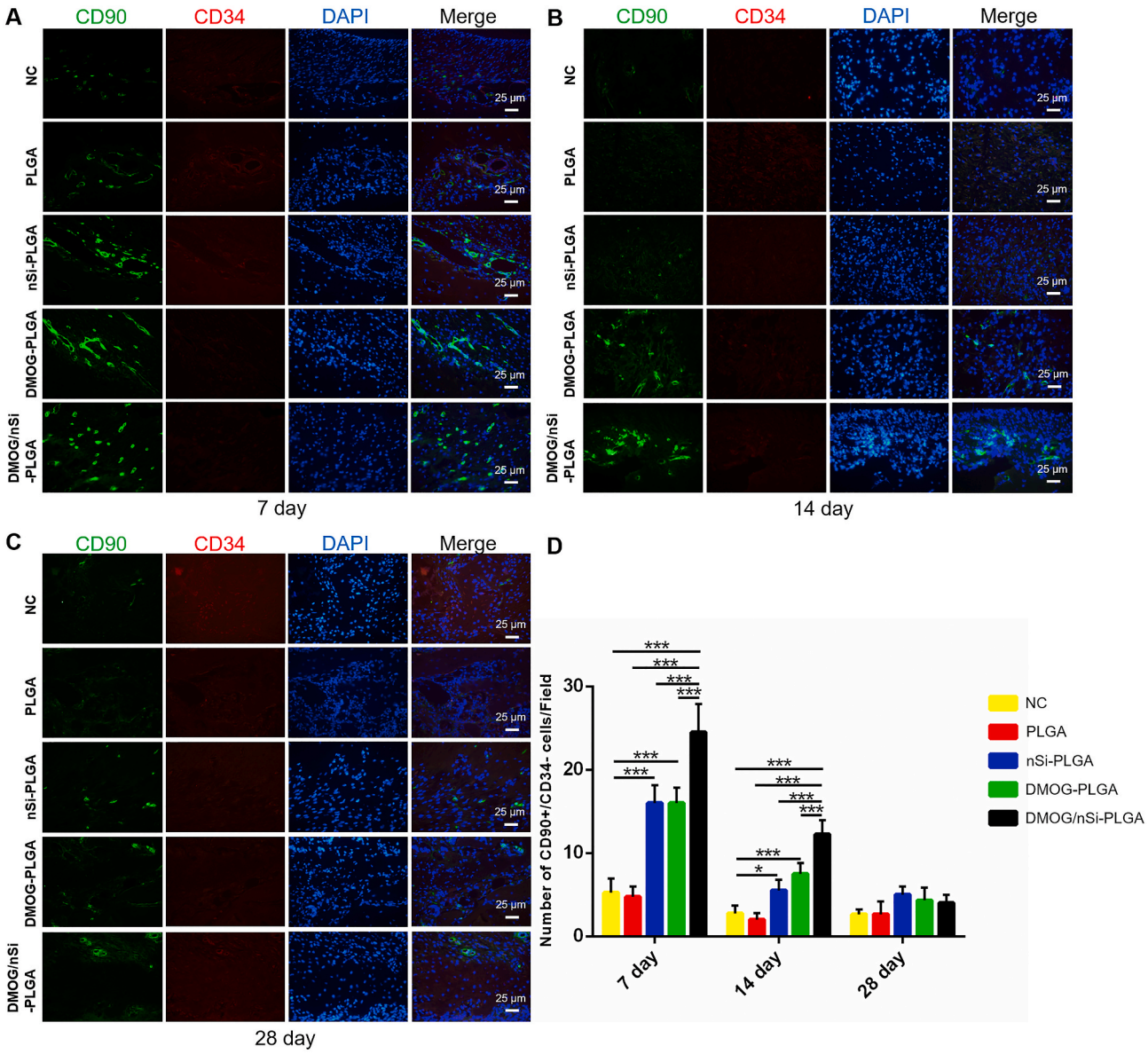

Fig. 4. Recruitment of stem cells in periodontal defects. (A–C) Immunofluorescent double staining for CD90+CD34− stromal cells in the periodontal defects at day 7, 21 and 28. Scale bars = 25 μm (D) Counting for the number of CD90+CD34− stromal cells (CD90+ cells: Green, CD34+ cells: Red). $^{*}p < 0.05$ and $^{***}p < 0.001$.

DMOG/nSi-PLGA group at week 8 was 49.63°, very comparable to that of mature periodontal ligament ($P > 0.05$). The angulations of other groups at week 4 and 8 were much smaller than that of native periodontal ligament (Fig. 6C, $P < 0.05$). Also, we found that the newly formed cementum in DMOG/nSi-PLGA group was thicker than that in the other groups, and no newly formed cementum was seen at week 4 in the other groups. Therefore, DMOG/nSi-PLGA fibrous membranes could promote cementum-periodontal ligament-bone complex repairing.

4. Discussion

In our study, based on orchestrating and enhancing osteogenesis-angiogenesis coupling, we prepared a DMOG/nSi-PLGA fibrous membranes for functional periodontal tissue regeneration. The physicochemical properties, releasing profile and cell compatibility were characterized. Both *in vitro* and *in vivo* studies were carried out to evaluate the effectiveness of the proposed design concept.

The prepared fibrous membranes with staggered fibrous structure had smooth morphology and well-distributed diameter. Incorporation of nSi could slightly decrease the diameter, which may be attributed to the enhanced electrical conductivity by nSi [16,17]. The element composition and content of nSi used for this study were coincident with a previous study [32]. The FTIR spectra of four membranes had similar characteristic peaks to those of the raw PLGA, which indicated that the functional groups and surface chemical properties did not change during the electrospinning process [30,31]. The unchanged surface chemical properties can prevent cellular regulation from being affected by the diversity of surface properties [33]. The mechanical property of tissue engineering materials is a critical element for cell survival, growth and tissue regeneration. The nSi-embedded fibrous membranes obtained the enhanced tensile strength and tensile modulus, which was in accordance with a previous study, and the possible explanation is that the incorporation of nSi augments the polymer crystallinity, interfacial area and interfacial bonding between organic and inorganic phases [34,35]. Therefore, the reinforced mechanical properties by nSi incorporation could guarantee sufficient mechanical loading ability of the electrospinning fibrous membranes. Electrospinning polymers have been served as sustained release vehicles of small molecules or

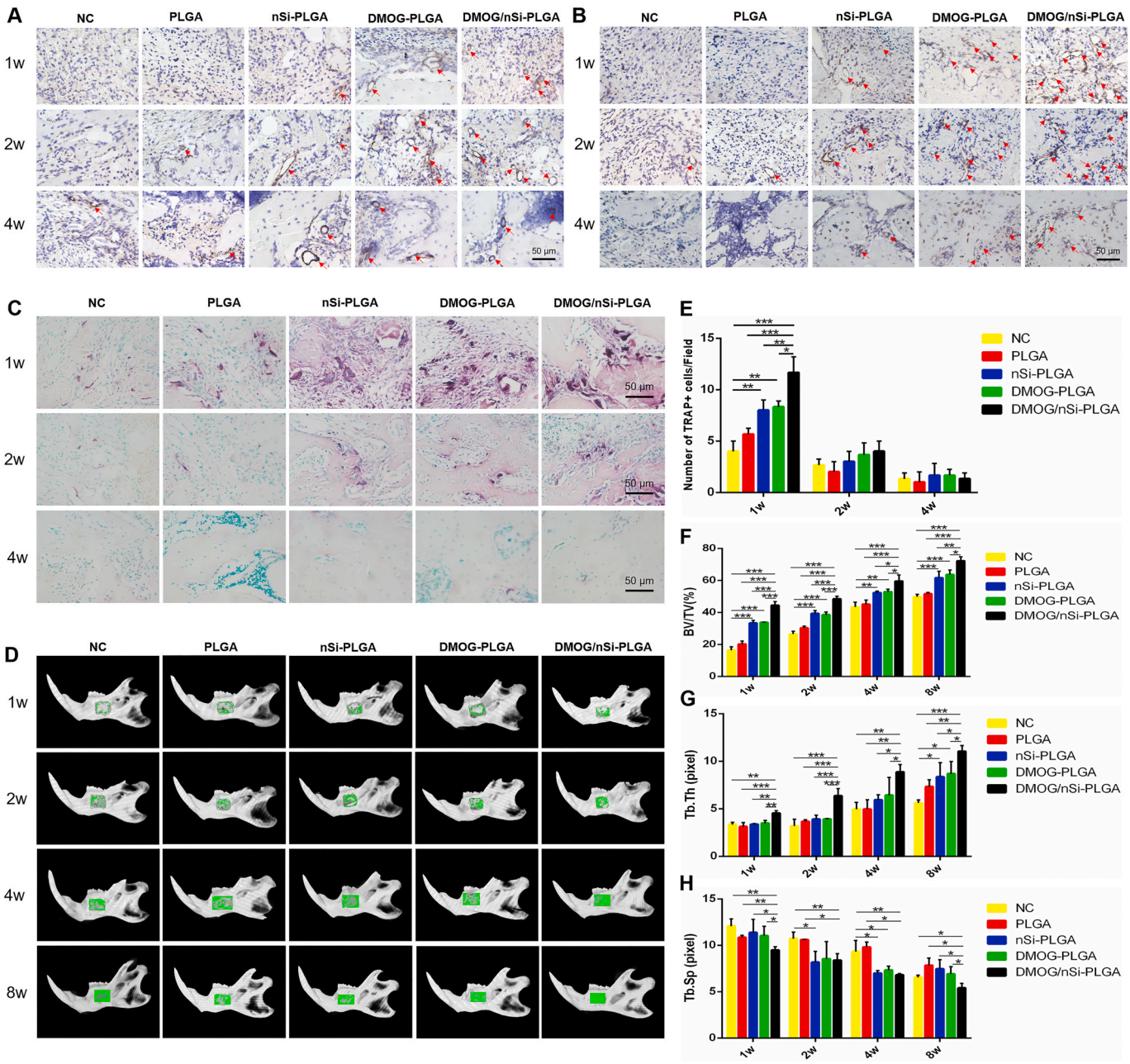

Fig. 5. Effects of DMOG/nSi-PLGA fibrous membranes on angiogenesis and alveolar bone remodeling *in vivo*. (A,B) Immunohistochemical staining of α-SMA (A) and CD31 (B) expression at week 1, 2 and 4 post-operation. The circular brown staining indicated blood vessels. (C) TRAP (red) staining representing osteoclastogenesis at week 1, 2 and 4 post-operation, and counting for the number of TRAP+ cells (E). (D,F–H) Micro-CT analysis of bone regeneration in mandibular defects at week 1, 2, 4 and 8 post-operation. (D) Representative 3D digital reconstructed planform images. Green color represented repair area in mandibular bone. (F–H) Quantitative analysis of the mandibular bone by reconstruction and analysis software. *$p < 0.05$, **$p < 0.01$, and ***$p < 0.001$. Scale bars = 50 μm.

macromolecules for biomedical applications [36]. Releasing profiles of DMOG and Si revealed the controlled releasing capacity of the PLGA polymeric fibers. The contact angle of PLGA fiber (138.1 ± 0.32°) was consistent with a previous study, and the reason for the biggest contact angle was that the stable water droplets were supported by the surface of the 3D fibrous construct with interconnected pores full of air [37]. The addition of DMOG and nSi could slightly improve the hydrophilicity of the polymer fibers, but the wettability of the fiber surface still affected cell attachment [38,39]. Therefore, the membranes were immersed in α-MEM overnight in advance to meliorate the hydrophilicity according to a previous study [40], which can provide a suitable surface wettability for cellular adhesion and spreading.

CLSM and SEM results indicated that the membranes could offer a compatible attachment surface for cell growth. Additionally, DMOG and nSi have been reported to be non-cytotoxic in a certain range of concentrations [15–17], and PLGA is a popular biocompatible polymer [28,29]. After cultivation with leach liquor, CCK-8 results showed high viability of PDLSCs, which conforms to the standard for cytocompatibility of biomaterials [32]. These results indicated that PLGA membranes with or without DMOG and nSi were cytocompatible and suitable for cell attachment and growth, which was in accordance with a previous study [41].

After osteogenic induction, DMOG/nSi-PLGA group presented the highest ALP activity and gene levels of osteogenesis-related markers among all groups. There was no significant difference for gene levels of Runx-2 and OPN at day 7. Previous studies also reported the discrepancy

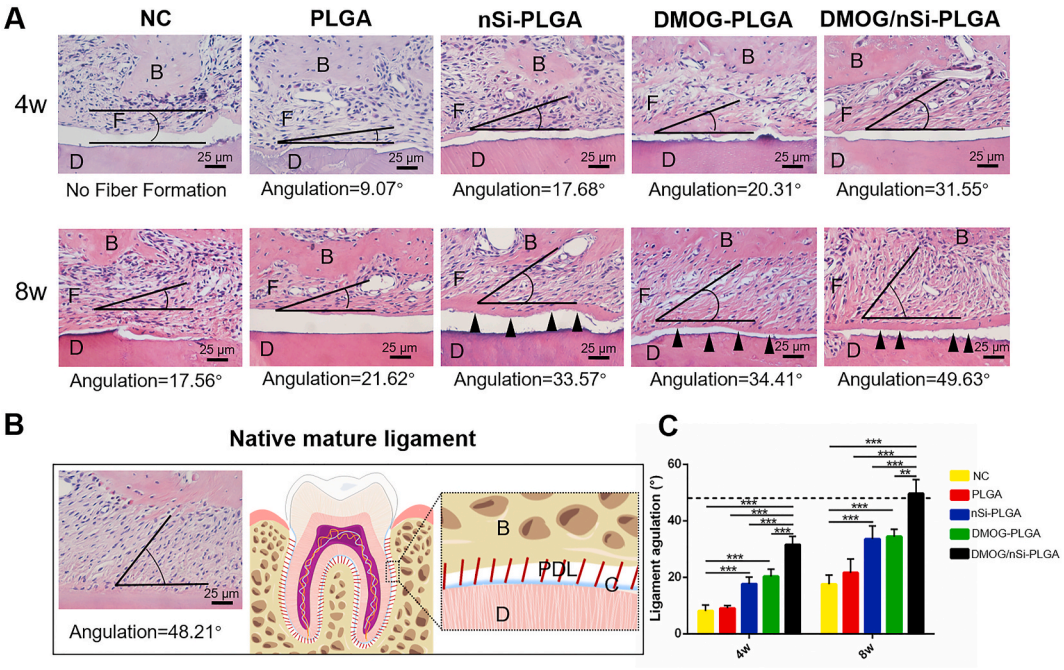

Fig. 6. Histological assessment for periodontal ligament and cementum regeneration. (A) H&E staining images of cementum-ligament-bone complex in periodontal defects at week 4 and 8 post-operation. Scale bars = 25 μm (B) H&E staining for the native ligament and corresponding schematic illustration. The black angles indicated the angulation of newly formed periodontal ligament. B, bone. F, regenerated fibers. D, dentine of the root. C, cementum. PDL, periodontal ligament. Black triangles represented newly formed cementum. (C) Analysis of the angular values of newly formed ligaments for all groups, and dotted line represented average angle of native mature ligament fibers. $^{**}p < 0.01$, and $^{***}p < 0.001$.

among different gene expression during osteogenic induction [42,43]. Transient increase of some osteogenic genes may be not found in early stage of osteogenic differentiation due to fewer time points settings (7, 14, and 21 days), and additional time point setting should be added to illuminate the gene expression pattern in different cellular cultivation conditions or substrates [42]. Overall, DMOG/nSi-PLGA fibrous membrane obtained a powerful effect on osteogenic differentiation of PDLSCs. As is well known, bone and blood vessels display spatial and functional relationships. Angiogenesis is another essential step for periodontal healing, due to the growth factors and nutrients brought by revascularization in the bone defects [44]. After validation of the pro-osteogenic potential of the DMOG/nSi-PLGA membranes, the angiogenic efficacy was explored. More obvious capillary-like networks were formed by cells on the DMOG/nSi-PLGA membranes. Previous studies showed that DMOG could enhance angiogenic activity of various cells [44–47]. Consistent with the cell tubule formation assay, the expression of the angiogenesis-related genes for cells cultured on DMOG/nSi-PLGA membranes was highest among all groups. Consequently, the angiogenesis assay illuminated that the DMOG/nSi-PLGA fibrous membranes was conducive to vascularization *in vitro*, which may provide the foundation for periodontal tissue regeneration.

With the favorable *in vitro* osteogenic and angiogenic effect, DMOG/nSi-PLGA fibrous membranes were implanted into periodontal defects of Wistar rats to investigate periodontal regeneration potential. Periodontal tissue or bone restoration is an intricate process involving highly orchestrated interactions between various cells and signals [48]. The recruitment of endogenous stromal cells is a pivotal step for *in situ* periodontal tissue engineering which contributes to wound healing and tissue regeneration by mobilizing and engrafting host own stem cells and precursor cells instead of transplantation of exogenous stem cells [49]. CD90+CD34− cells were regarded as non-hematopoietic stem and progenitor cells according to a previous study [49]. Our findings indicated that DMOG/nSi-PLGA fibrous membranes exerted the strongest chemotactic effect in early stage of tissue healing, which is beneficial to the enhancement of stromal cells migration and periodontal tissue regeneration, and the exact underneath mechanism remains unclear and needs further study to address. DMOG-activated HIF pathway could mediate MSCs migration by upregulating the expression of chemokine receptors CXCR4 and vascular endothelial growth factor receptor 1 (VEGFR1) [50]. With regard to nSi, enhanced recruitment effect may be ascribed to the dissociated Mg^{2+} upregulating VEGF expression [21].

Revascularization is a prerequisite for the formation of functional tissue since vessel in-growth not only supplies oxygen and nutrients, but also provides access for cell circulation in favor of damaged periodontium restoration [6,51]. α-SMA, expressed at vascular wall, contributes to the formation of vascular smooth muscle cell cytoskeleton [52]. CD31, existing in endothelial cell junction, is involved in sustaining the function of vascular endothelial barrier [53]. Immunohistochemical staining for α-SMA and CD31 showed that DMOG/nSi-PLGA groups exhibited a higher level of angiogenic marker expression and neovascularization *in vivo* at early wound healing (at week 1 and 2), which was consistent with previous studies [44–47]. In our study, DMOG/nSi-PLGA fibrous membranes could stimulate *in vitro* angiogenic differentiation and enhance *in vivo* angiogenesis, thereby providing a favorable blood supply for restoration of periodontal damages. Consequently, DMOG/nSi-PLGA fibrous membranes may promote periodontal tissue regeneration by enhancing angiogenesis in periodontal defects.

Active osteoclast activities appeared in the early phase of wound repairing, and the balance between osteoblasts and osteoclasts can maintain the structural integrity of bone during bone remodeling. Generally, bone resorption sites tend to attract osteogenic precursors and express high levels of bone matrix proteins for osteogenic differentiation [49]. DMOG/nSi-PLGA fibrous membranes inspired early transient osteoclastogenesis, thereby regulating osteoblast activities indirectly since osteoclast activity and osteoblast activity are intertwined in the process of bone metabolism [49]. Micro-CT and H&E staining were carried out to assess osteogenic effect of DMOG/nSi-PLGA fibrous membranes on periodontal defect repairing. Numerous studies demonstrated that DMOG contributed effectively to bone regeneration *in vivo* via enhanced vascularization [44,47,54]. The osteogenic effect of

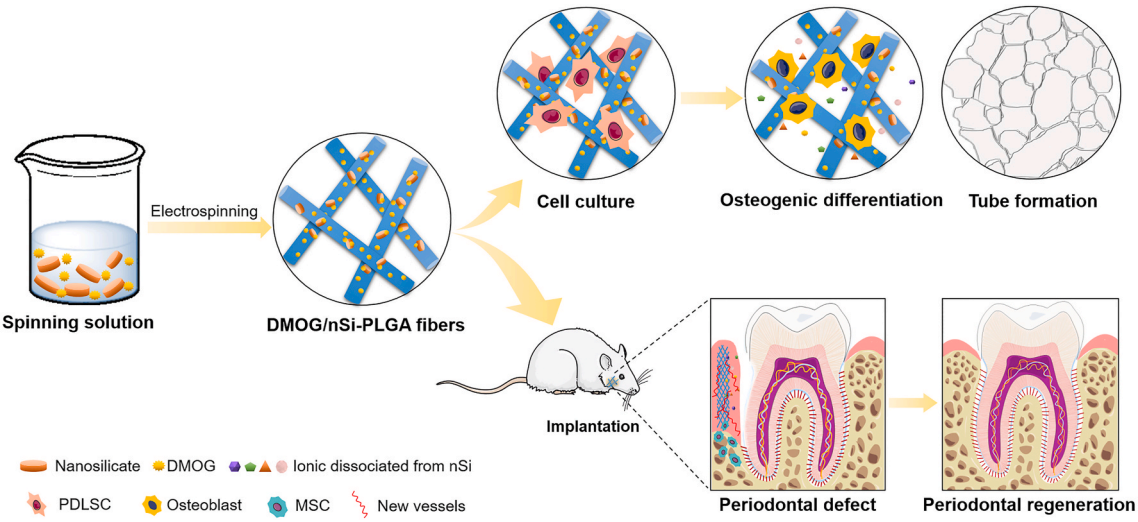

Scheme 1. Schematics for the process of material preparation and periodontal tissue regeneration. Partial elements were from the Smart Servier Medical Art, available from https://smart.servier.com/image-set-download/and licensed under a Creative Common Attribution 3.0 Generic License. http://smart.servier.com/.

nSi has been widely verified in diverse cell types [17,25–27,55,56] whereas its roles in *in situ* osteogenesis especially periodontal bone regeneration has rarely been reported. In our study, DMOG and nSi improved the periodontal bone remodeling respectively, but the combination of the two bioactive factors positively maximized periodontal bone regeneration. Further, bone specific matrix protein levels were detected by immunohistochemical staining. ALP is considered as an early marker of osteoblast phenotype and osteogenesis differentiation [57]. Runx-2 is an essential osteogenic transcription factor for osteoblast differentiation and osteogenic gene expression [57,58]. As the main extracellular matrix protein of bone, Col-I stimulates osteoblast adhesion and differentiation [57]. The DMOG/nSi-PLGA fibrous membranes significantly up-regulated the levels of these osteogenic differentiation-related proteins, and thereby forcefully confirmed the collaborative effect of DMOG and nSi on periodontal bone regeneration.

Periodontal tissue regeneration requires the functional restoration of the primary structure of cementum-periodontal ligament-alveolar bone complex, which ensures the functional stability and biomechanical loading of periodontium [59]. DMOG/nSi-PLGA membrane could improve ligament fiber orientation thereby forming mature functional periodontal ligament which is conductive to supporting and loading [49]. The fibrous membrane enhanced the recruitment of stem cells and angiogenesis, which was conducive to bone regeneration, and it was also possible that stem cells engraftment and angiogenesis facilitated the regeneration and orientation of periodontal ligament [60–62]. 3D pore construct has been reported to promote the restoration of periodontal complex [59,60]. The 3D fibrous structure of the membranes with interconnected pores, on the other hand, may be in favor of oriented periodontal ligament formation. Further study should be implemented to address the exact mechanism. Additionally, DMOG/nSi-PLGA group acquired appropriate thickness newly formed cementum. Therefore, DMOG/nSi-PLGA membrane promoted the regeneration of functional periodontium as evidenced by the restoration of cementum-periodontal ligament-bone complex.

In summary, we successfully prepared electrospinning DMOG/nSi-PLGA fibrous membranes based on the principle of orchestrating the coupled process of osteogenesis-angiogenesis. The DMOG/nSi-PLGA membranes was capable of inducing osteogenic differentiation of PDLSCs, and promoting capillary-like tube formation *in vitro*. By recruiting CD90+/CD34− stromal cells and promoting the osteogenesis and revascularization of periodontal defect, the difunctional membranes facilitated the functional periodontal tissue regeneration (Scheme 1). Furthermore, the needs of alleviating inflammatory responses and anti-infection are indispensable for the scaffolds since periodontitis is an infectious inflammatory disease. Therefore, in the follow-up study, the immunomodulation and anti-infection effects of the fibrous membranes will be addressed to facilitate periodontal tissue regeneration.

5. Conclusions

In this study, a difunctional DMOG/nSi-PLGA fibrous membrane was prepared to orchestrate and enhance osteogenesis-angiogenesis coupling for optimal periodontal regeneration. The embedded nSi endowed the fibrous membranes with better tensile strength and modulus. The membranes possessed good biocompatibility in favor of cell adhesion and growth. Importantly, the DMOG/nSi-PLGA fibrous membrane had powerful effects on osteogenic and angiogenic differentiation of PDLSCs in comparison with single-loaded membranes. After implanted into periodontal defects, the DMOG/nSi-PLGA fibrous membranes obtained satisfactory periodontal defect restoration by recruitment of CD90+/CD34− stromal cells, promotion of angiogenesis, and regulation of bone remodeling, as well as ultimate formation of functional cementum-periodontal ligament-bone complex. The cooperative application of DMOG and nSi achieved the optimal promotion effects, and the favorable stabilities of small molecules and nanomaterials determine small doses and low cost in favor of mass production. Therefore, the combination of DMOG and nSi could be a prospective strategy for periodontal tissue regeneration, and the difunctional fibrous structure also provide a promising scaffold for regenerative medicine.

CRediT authorship contribution statement

Lingling Shang: Data curation, Formal analysis, Methodology, Software, Validation, Writing - original draft. **Ziqi Liu:** Methodology, Software, Writing - review & editing. **Baojin Ma:** Conceptualization, Writing - review & editing. **Jinlong Shao:** Conceptualization, Writing - review & editing. **Bing Wang:** Conceptualization, Writing - review & editing. **Chenxi Ma:** Software, Formal analysis. **Shaohua Ge:** Conceptualization, Funding acquisition, Resources, Supervision, Writing - review & editing.

Declaration of competing interest

The authors declare that they have no known competing financial interests or personal relationships that could have appeared to influence the work reported in this paper.

Acknowledgments

This research was supported by the National Natural Science Foundation of China (No. 81670993, 81873716, and 81901009), The Construction Engineering Special Fund of "Taishan Scholars" of Shandong Province (No.ts20190975 and tsqn201909180), National Key R&D Program of China (No. 2017YFB0405400), Collaborative Innovation Center of Technology and Equipment for Biological Diagnosis and Therapy in Universities of Shandong, The National Key Research and Development Program of China (No. 2017YFA0104604), Open Foundation of Shandong Provincial Key Laboratory of Oral Tissue Regeneration (No. SDKQ201901, SDKQ201904). The funders had no role in study design, data collection and analysis, decision to publish or preparation of the manuscript. The authors also thank Prof. Hongyu Zhang and Dr. Yi Wang from Tsinghua University for technical guidance. The authors declare that no financial or other potential competing interests exist with regard to this study.

Appendix A. Supplementary data

Supplementary data to this article can be found online at https://doi.org/10.1016/j.bioactmat.2020.10.010.

References

[1] E. Kononen, M. Gursoy, U.K. Gursoy, Periodontitis: a multifaceted disease of tooth-supporting tissues, J. Clin. Med. 8 (8) (2019) 1135.
[2] C. Manresa, E.C. Sanz-Miralles, J. Twigg, et al., Supportive periodontal therapy (SPT) for maintaining the dentition in adults treated for periodontitis, Cochrane Database Syst. Rev. 1 (2018) CD009376.
[3] Z. Liu, X. Yin, Q. Ye, et al., Periodontal regeneration with stem cells-seeded collagen-hydroxyapatite scaffold, J. Biomater. Appl. 31 (1) (2016) 121–131.
[4] H. Xie, Z. Gu, C. Li, et al., A novel bioceramic scaffold integrating silk fibroin in calcium polyphosphate for bone tissue-engineering, Ceram. Int. 42 (2) (2016) 2386–2392.
[5] Y. Kuroda, T. Kawai, K. Goto, et al., Clinical application of injectable growth factor for bone regeneration: a systematic review, Inflamm. Regen. 39 (2019) 20.
[6] X. Qi, Y. Liu, Z.Y. Ding, et al., Synergistic effects of dimethyloxallyl glycine and recombinant human bone morphogenetic protein-2 on repair of critical-sized bone defects in rats, Sci. Rep. 7 (2017) 42820.
[7] K.M. Woo, H.M. Jung, J.H. Oh, et al., Synergistic effects of dimethyloxalylglycine and butyrate incorporated into alpha-calcium sulfate on bone regeneration, Biomaterials 39 (2015) 1–14.
[8] G.L. Semenza, Targeting hypoxia-inducible factor 1 to stimulate tissue vascularization, J. Invest. Med. 64 (2) (2016) 361–363.
[9] Q. Zhang, J.H. Oh, C.H. Park, et al., Effects of dimethyloxalylglycine-embedded poly(epsilon-caprolactone) fiber meshes on wound healing in diabetic rats, ACS Appl. Mater. Interfaces 9 (9) (2017) 7950–7963.
[10] X. Ren, Y. Han, J. Wang, et al., An aligned porous electrospun fibrous membrane with controlled drug delivery - an efficient strategy to accelerate diabetic wound healing with improved angiogenesis, Acta Biomater. 70 (2018) 140–153.
[11] Z. Min, Z. Shichang, X. Chen, et al., 3D-printed dimethyloxallyl glycine delivery scaffolds to improve angiogenesis and osteogenesis, Biomater. Sci. 3 (8) (2015) 1236–1244.
[12] H. Ding, Y.S. Gao, Y. Wang, et al., Dimethyloxaloylglycine increases the bone healing capacity of adipose-derived stem cells by promoting osteogenic differentiation and angiogenic potential, Stem Cell. Dev. 23 (9) (2014) 990–1000.
[13] M. Shi, Y. Zhou, J. Shao, et al., Stimulation of osteogenesis and angiogenesis of hBMSCs by delivering Si ions and functional drug from mesoporous silica nanospheres, Acta Biomater. 21 (2015) 178–189.
[14] P. Fraisl, J. Aragones, P. Carmeliet, Inhibition of oxygen sensors as a therapeutic strategy for ischaemic and inflammatory disease, Nat. Rev. Drug Discov. 8 (2) (2009) 139–152.
[15] L. Shang, T. Wang, D. Tong, et al., Prolyl hydroxylases positively regulated LPS-induced inflammation in human gingival fibroblasts via TLR4/MyD88-mediated AKT/NF-kappaB and MAPK pathways, Cell Prolif 51 (6) (2018), e12516.
[16] H. Tomas, C.S. Alves, J. Rodrigues, R. Laponite, A key nanoplatform for biomedical applications? Nanomedicine 14 (7) (2018) 2407–2420.
[17] A.K. Gaharwar, L.M. Cross, C.W. Peak, et al., 2D nanoclay for biomedical applications: regenerative medicine, therapeutic delivery, and additive manufacturing, Adv. Mater. 31 (23) (2019), e1900332.
[18] A. Hoppe, N.S. Guldal, A.R. Boccaccini, A review of the biological response to ionic dissolution products from bioactive glasses and glass-ceramics, Biomaterials 32 (11) (2011) 2757–2774.
[19] D.M. Reffitt, N. Ogston, R. Jugdaohsingh, et al., Orthosilicic acid stimulates collagen type 1 synthesis and osteoblastic differentiation in human osteoblast-like cells in vitro, Bone 32 (2) (2003) 127–135.
[20] C.C. Hung, A. Chaya, K. Liu, et al., The role of magnesium ions in bone regeneration involves the canonical Wnt signaling pathway, Acta Biomater. 98 (2019) 246–255.
[21] S. Yoshizawa, A. Brown, A. Barchowsky, et al., Role of magnesium ions on osteogenic response in bone marrow stromal cells, Connect. Tissue Res. 55 (Suppl 1) (2014) 155–159.
[22] C.R.H.H. Zreiqat, A. Zannettino, P. Evans, G. Schulze-Tanzil, C. Knabe, M. Shakibaei, Mechanisms of magnesium-stimulated adhesion of osteoblastic cells to commonly used orthopaedic implants, J. Biomed. Mater. Res. 62 (2) (2002) 175–184.
[23] M.A. Philippe Clément-Lacroix, Frederic morvan, sergio roman-roman, Béatrice Vayssière, cecille Belleville, kenneth Estrera, matthew L Warman, roland Baron, Georges rawadi, Lrp5-independent activation of Wnt signaling by lithium chloride increases bone formation and bone mass in mice, Proc. Natl. Acad. Sci. U. S. A. 102 (48) (2005) 17406–17411.
[24] F. Zhang, C.J. Phiel, L. Spece, et al., Inhibitory phosphorylation of glycogen synthase kinase-3 (GSK-3) in response to lithium. Evidence for autoregulation of GSK-3, J. Biol. Chem. 278 (35) (2003) 33067–33077.
[25] S.M. Mihaila, A.K. Gaharwar, R.L. Reis, et al., The osteogenic differentiation of SSEA-4 sub-population of human adipose derived stem cells using silicate nanoplatelets, Biomaterials 35 (33) (2014) 9087–9099.
[26] T. Li, Z.L. Liu, M. Xiao, et al., Impact of bone marrow mesenchymal stem cell immunomodulation on the osteogenic effects of laponite, Stem Cell Res. Ther. 9 (1) (2018) 100.
[27] A.K. Gaharwar, S.M. Mihaila, A. Swami, et al., Bioactive silicate nanoplatelets for osteogenic differentiation of human mesenchymal stem cells, Adv. Mater. 25 (24) (2013) 3329–3336.
[28] M. Mir, N. Ahmed, A.u. Rehman, Recent applications of PLGA based nanostructures in drug delivery, Colloids Surf. B Biointerfaces 159 (2017) 217–231.
[29] R.K. Deepak N Kapoor, Bhatia Amit, Ruchi Sharma, et al., PLGA: a unique polymer for drug delivery, Ther. Deliv. 6 (1) (2015) 41–58.
[30] T.S.J.K.R. Masaeli, R. Dinarvand, M. Tahriri, et al., Preparation, characterization and evaluation of drug release properties of simvastatin-loaded PLGA microspheres, Iran. J. Pharm. Res. (IJPR) 15 (Suppl) (2016) 205–211.
[31] R.K. Kankala, X.M. Xu, C.G. Liu, et al., 3D-Printing of microfibrous porous scaffolds based on hybrid approaches for bone tissue engineering, Polymers 10 (7) (2018).
[32] Y. Wang, W. Cui, J. Chou, et al., Electrospun nanosilicates-based organic/inorganic nanofibers for potential bone tissue engineering, Colloids Surf B: Biointerfaces 172 (2018) 90–97.
[33] B. Ma, S. Zhang, F. Liu, et al., One-dimensional hydroxyapatite nanostructures with tunable length for efficient stem cell differentiation regulation, ACS Appl. Mater. Interfaces 9 (39) (2017) 33717–33727.
[34] J.D. Mackenzie, Q. Huang, T. Iwamoto, Mechanical properties of ormosils, J. Sol. Gel Sci. Technol. 7 (1996) 151–161.
[35] G. Poologasundarampillai, B. Yu, J.R. Jones, et al., Electrospun silica/PLLA hybrid materials for skeletal regeneration, Soft Matter 7 (21) (2011) 10241–10251.
[36] R. Contreras-Caceres, L. Cabeza, G. Perazzoli, et al., Electrospun nanofibers: recent applications in drug delivery and cancer therapy, Nanomaterials 9 (4) (2019).
[37] Y. Qian, H. Chen, Y. Xu, et al., The preosteoblast response of electrospinning PLGA/PCL nanofibers: effects of biomimetic architecture and collagen I, Int. J. Nanomed. 11 (2016) 4157–4171.
[38] S.H. Ku, J. Ryu, S.K. Hong, et al., General functionalization route for cell adhesion on non-wetting surfaces, Biomaterials 31 (9) (2010) 2535–2541.
[39] Y. Arima, H. Iwata, Effect of wettability and surface functional groups on protein adsorption and cell adhesion using well-defined mixed self-assembled monolayers, Biomaterials 28 (2007) 3074–3082.
[40] X. Li, B. Ma, J. Li, et al., A method to visually observe the degradation-diffusion-reconstruction behavior of hydroxyapatite in the bone repair process, Acta Biomater. 101 (2020) 554–564.
[41] Z. Wang, J. Hu, J. Yu, et al., Preparation and characterization of nano-laponite/PLGA composite scaffolds for urethra tissue engineering, Mol. Biotechnol. 62 (3) (2020) 192–199.
[42] C. Zhao, Q. Chen, S. Yu, et al., Effect of interleukin-22 on osteogenic differentiation and the osteoclastogenic response of human periodontal ligament fibroblasts in vitro, J. Periodontol. 91 (8) (2020) 1085–1097.
[43] B. Ge, H. Liu, Q. Liang, et al., Oxytocin facilitates the proliferation, migration and osteogenic differentiation of human periodontal stem cells in vitro, Arch. Oral Biol. 99 (2019) 126–133.
[44] J. Zhang, J. Guan, X. Qi, et al., Dimethyloxaloylglycine promotes the angiogenic activity of mesenchymal stem cells derived from iPSCs via activation of the PI3K/akt pathway for bone regeneration, Int. J. Biol. Sci. 12 (6) (2016) 639–652.
[45] S.M. Kim, Q. Li, J.H. An, et al., Enhanced angiogenic activity of dimethyloxalylglycine-treated canine adipose tissue-derived mesenchymal stem cells, J. Vet. Med. Sci. 81 (11) (2019) 1663–1670.
[46] T. Kifune, H. Ito, M. Ishiyama, et al., Hypoxia-induced upregulation of angiogenic factors in immortalized human periodontal ligament fibroblasts, J. Oral Sci. 60 (4) (2018) 519–525.
[47] B. Liang, J.M. Liang, J.N. Ding, et al., Dimethyloxaloylglycine-stimulated human bone marrow mesenchymal stem cell-derived exosomes enhance bone regeneration through angiogenesis by targeting the AKT/mTOR pathway, Stem Cell Res. Ther. 10 (1) (2019) 335.
[48] A. Grosso, M.G. Burger, A. Lunger, et al., It takes two to tango: coupling of angiogenesis and osteogenesis for bone regeneration, Front. Bioeng. Biotechnol. 5 (2017) 68.

[49] F. Wang, L. Du, S. Ge, PTH/SDF-1 alpha cotherapy induces CD90+CD34- stromal cells migration and promotes tissue regeneration in a rat periodontal defect model, Sci. Rep. 6 (2016) 30403.
[50] L. Fan, J. Li, Z. Yu, et al., The hypoxia-inducible factor pathway, prolyl hydroxylase domain protein inhibitors, and their roles in bone repair and regeneration, BioMed Res. Int. 2014 (2014) 239356.
[51] E. Schipani, C. Maes, G. Carmeliet, et al., Regulation of osteogenesis-angiogenesis coupling by HIFs and VEGF, J. Bone Miner. Res. 24 (8) (2009) 1347–1353.
[52] Y. Sun, Z. Yang, B. Zheng, et al., A novel regulatory mechanism of smooth muscle alpha-actin expression by NRG-1/circACTA2/miR-548f-5p Axis, Circ. Res. 121 (6) (2017) 628–635.
[53] P. Lertkiatmongkol, D. Liao, H. Mei, et al., Endothelial functions of platelet/endothelial cell adhesion molecule-1 (CD31), Curr. Opin. Hematol. 23 (3) (2016) 253–259.
[54] J. Peng, Z.G. Lai, Z.L. Fang, et al., Dimethyloxalylglycine prevents bone loss in ovariectomized C57BL/6J mice through enhanced angiogenesis and osteogenesis, PLoS One 9 (11) (2014), e112744.
[55] J.K. Carrow, L.M. Cross, R.W. Reese, et al., Widespread changes in transcriptome profile of human mesenchymal stem cells induced by two-dimensional nanosilicates, Proc. Natl. Acad. Sci. U. S. A. 115 (17) (2018) E3905–E3913.
[56] G. Cidonio, M. Cooke, M. Glinka, et al., Printing bone in a gel: using nanocomposite bioink to print functionalised bone scaffolds, Mater. Today Bio 4 (2019) 100028.
[57] J. An, H. Yang, Q. Zhang, et al., Natural products for treatment of osteoporosis: the effects and mechanisms on promoting osteoblast-mediated bone formation, Life Sci. 147 (2016) 46–58.
[58] T. Komori, Regulation of proliferation, differentiation and functions of osteoblasts by Runx 2, Int. J. Mol. Sci. 20 (7) (2019).
[59] C.H. Park, H.F. Rios, Q. Jin, et al., Tissue engineering bone-ligament complexes using fiber-guiding scaffolds, Biomaterials 33 (1) (2012) 137–145.
[60] J. Liu, J. Ruan, M.D. Weir, et al., Periodontal bone-ligament-cementum regeneration via scaffolds and stem cells, Cells 8 (6) (2019) 537.
[61] K. Kim, C.H. Lee, B.K. Kim, et al., Anatomically shaped tooth and periodontal regeneration by cell homing, J. Dent. Res. 89 (8) (2010) 842–847.
[62] W. Zhu, Q. Zhang, Y. Zhang, et al., PDL regeneration via cell homing in delayed replantation of avulsed teeth, J. Transl. Med. 13 (2015) 357.